On the Sn loss from thin films of the material system Cu–Zn–Sn–S in high vacuum

A. Weber,[a)] R. Mainz, and H. W. Schock
Helmholtz-Zentrum Berlin für Materialien und Energie, Glienicker Str. 100, D-14109 Berlin, Germany

In this paper the Sn loss from thin films of the material system Cu–Zn–Sn–S and the subsystems Cu–Sn–S and Sn–S in high vacuum is investigated. A combination of *in situ* x-ray diffractometry and x-ray fluorescence (XRF) at a synchrotron light source allowed identifying phases, which tend to decompose and evaporate a Sn-containing compound. On the basis of the XRF results a quantification of the Sn loss from the films during annealing experiments is presented. It can be shown that the evaporation rate from the different phases decreases according to the order $SnS \rightarrow Cu_2SnS_3 \rightarrow Cu_4SnS_4 \rightarrow Cu_2ZnSnS_4$. The phase SnS is assigned as the evaporating compound. The influence of an additional inert gas component on the Sn loss and on the formation of Cu_2ZnSnS_4 thin films is discussed. © *2010 American Institute of Physics*. [doi:10.1063/1.3273495]

I. INTRODUCTION

The compound semiconductor Cu_2ZnSnS_4 has gained interest in the past years as its physical properties make it suitable as an absorber material for thin film photovoltaic devices.[1,2] Its crystalline structure is commonly referred to as the kesterite type.[3–5] This structure is strongly related to the chalcopyrite structure of the well known photovoltaic absorber material $Cu(In,Ga)Se_2$.[6] Starting from $Cu(In,Ga)Se_2$ the kesterite structure can be obtained by replacing In and Ga with Zn and Sn and Se with S. Such a replacement may be interesting as Zn, Sn, and S are much more abundant in Earth's crust than In, Ga, and Se. Up to now the best solar cells based on Cu_2ZnSnS_4 are formed by annealing metallic and sulfidic precursor layers in a sulfur containing atmosphere for several hours. These absorbers reach energy conversion efficiencies of 6.7%.[2] The efficiency and also the long processing times are still unsatisfactory. Some attempts[7–10] have been made to use physical vapor deposition (PVD), which is successfully used for the deposition of $Cu(In,Ga)Se_2$,[11] to shorten growth times and to improve process control and process reproducibility. In an earlier work[9] we found in accordance with Ref. 7 that the Sn content of the layers decreases with increasing substrate temperatures during such a PVD process. This effect may be explained either by a decreasing adsorption of Sn atoms on the substrate surface or by the re-evaporation of Sn or a Sn compound from the deposited layer. In this work we investigate the latter possibility on the basis of an experimental series on precursor layers of the material systems Sn–S, Cu–Sn–S, and Cu–Zn–Sn–S. We detect changes in the elemental composition and the phase composition during a heating experiment by a combination of *in situ* x-ray fluorescence (XRF) and x-ray diffraction (XRD). We will discuss how the x-ray signals can be used for the quantitative evaluation of the Sn content of the layers and the influence of an additional gas atmosphere on the Sn loss at elevated temperatures.

a)Electronic mail: alfons.weber@helmholtz-berlin.de.

II. EXPERIMENTAL

Precursor layers were deposited on Mo-coated soda-lime glass substrates in a PVD system with elemental sources of Cu, Sn, and S and binary sources of ZnS and SnS. The PVD system allowed depositing layered films of different binary sulfides as well as homogeneously coevaporated films. Thin films of the three different material systems Sn–S, Cu–Sn–S, and Cu–Zn–Sn–S were prepared. The material amounts of all films were aimed for a 2 μm thick layer of Cu_2ZnSnS_4. The evaporation rate was measured by a calibrated quartz crystal monitor. The error of the measurement is approximated to be less than 15%. Table I gives an overview of the different film types. For each material system two types of precursors were grown: one with a homogeneously coevaporated film and one with a layered film. The layered films were of the sequence glass/Mo/SnS/CuS/ZnS. This sequence was used to evaluate the effect of covering the Sn-containing part of the film on the Sn loss from the layers.

The Sn-loss experiments on these precursors were carried out in a vacuum chamber equipped with a heatable substrate stage and a Knudsen-type sulfur source (S-source). The base pressure of the chamber was approximately 1×10^{-3} Pa. During the Sn-loss experiment the S-source was operated at a temperature of 180 °C, which leads to a chamber pressure of 1×10^{-2} Pa. The heating of the sulfur source started 20 min before the substrate was heated to assure a

TABLE I. Overview of different investigated precursors (slashes mark the interfaces, and coevaporated elements are catenated with "+"). The Sn amount was derived from the Sn-deposition rate.

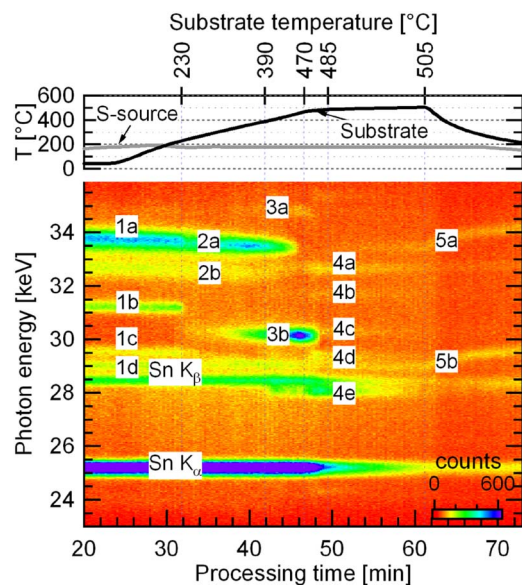| Layer structure	Sn amount (at./cm^2)
Mo/Sn+S	1.2×10^{18}
Mo/Cu+Sn+S	1.1×10^{18}
Mo/Cu+Zn+Sn+S	1.0×10^{18}
Mo/SnS	1.1×10^{18}
Mo/SnS/Cu+S	1.1×10^{18}
Mo/SnS/Cu+S/ZnS	1.1×10^{18}

FIG. 1. (Color online) Two-dimensional representation of the detected energy dispersive signals (bottom part of the graph) during the heating program (top part of the graph) on a precursor of the structure Mo/SnS/CuS. The following phases can be identified: CuS (Ref. 13) [(1a) hkl=103, (1b) 102, (1c) 101, and (1d) 100], SnS (Ref. 14) [(2a) 111 and (2b) 101], Cu_2SnS_3 (Ref. 15) [(3a) 131 and (3b) −131], Cu_4SnS_4 (Ref. 16) [(4a) 112, (4b) 221, (4c) 102, (4d) 121, and (4e) 220], and $Cu_{2-x}S$ (Ref. 17) [(5a) 200 and (5b) 111].

constant S-pressure. The pressure was measured by a Bayard–Alpert hot cathode vacuum gauge attached to the vacuum chamber. In the standard experiment the substrate was heated for 25 min from room temperature to a nominal temperature of 550 °C. The nominal temperature was measured by a thermocouple in the heating zone; the temperature of the thin film was measured by a Pt100 attached to the substrate surface. All further temperature values will refer to the Pt100 measurement unit.

The vacuum chamber was mounted on the beamline F3 of the HASYLAB synchrotron source. Polychromatic synchrotron radiation enters through a polyimide window and interacts with the film. Under an angle 2Θ of 7.5° the diffraction and fluorescence signals exit the chamber through a second polyimide window and are detected energy dispersively in the energy range between 5 and 55 keV. Every 15 s a complete spectrum is recorded, which allows for a high time resolution of the signals during the experiment. Further details on the measurement setup can be found elsewhere.[12]

Scanning electron microscopy (SEM) micrographs and depth profiling by energy dispersive x-ray spectroscopy (EDX) were carried out on a Leo 1350 with a field emission cathode. The acceleration voltage for EDX was 8 keV; thus only the L-lines of the metals were analyzed.

III. RESULTS

All precursors were analyzed during an identical heating program as described in Sec. II. Figure 1 shows the experimental data recorded during the heating experiment on a precursor of the structure Mo/SnS/CuS. The energy range from 23 to 36 keV was selected to give an overview of all crystalline phases appearing during the experiment and the

TABLE II. List of phases that could be identified by XRD during the heating experiments for various precursor types. The diffraction signals of phases marked with an asterisk "*" disappear irreversibly in the course of the experiment. The diffraction signals of ZnS, Cu_2SnS_3, and Cu_2ZnSnS_4 may overlap, and these phases are therefore combined in parentheses.

Precursor	List of phases (and their temperature ranges in °C)
Mo/Sn+S	SnS_2 (20–360)*
	Sn_2S_3 (320–380)*
	SnS (330–410)*
Mo/Cu+Sn+S	Cu_2SnS_3 (20–470)*
	Cu_4SnS_4 (400–500)*
	$Cu_{2-x}S$ (480–505)
Mo/Cu+Zn+Sn+S	[ZnS/Cu_2SnS_3/Cu_2ZnSnS_4] (20–505)
Mo/SnS	SnS (20–480)*
	Sn_2S_3 (320–380)*
Mo/SnS/CuS	CuS (20–230)
	SnS (20–470)*
	$Cu_{2-x}S$ (230–505)
	Cu_2SnS_3 (20–485)*
	Cu_4SnS_4 (390–505)
Mo/SnS/CuS/ZnS	CuS (20–350)
	SnS (20–470)*
	$Cu_{2-x}S$ (350–505)
	[ZnS/Cu_2SnS_3/Cu_2ZnSnS_4] (20–505)

development of the Sn K fluorescence lines. During the experiment the ternary phases Cu_2SnS_3 and Cu_4SnS_4 form and the intensity of the Sn $K\alpha$ fluorescence line decreases significantly.

Table II gives an overview of the development of phases for this and all other investigated precursors according to the detected diffraction signals. For the two precursors of the material system Sn–S all diffraction signals of the film decrease below the detection limit in the course of the heating experiment. In both precursor types of the system Cu–Sn–S the phase Cu_2SnS_3 appears first and Cu_4SnS_4 second. As in the case of the Sn–S phases the diffraction intensity of these phases falls below the detection limit within the heating experiment.

In the system Cu–Zn–Sn–S the diffraction signals of the phase Cu_2ZnSnS_4 cannot be distinguished from the phases ZnS (sphalerite) and Cu_2SnS_3 due to their structural similarity.[18] The diffraction peaks of these phases can overlap, and, for a more comprehensible representation, these peaks will be called Σ-signals in this paper, with the hkl-indices of the cubic sphalerite structure. Nevertheless we found significant differences in the film formation of the Cu–Sn–S and the Cu–Zn–Sn–S system. Figure 2 shows the deviations in the evolution of the Sn $K\alpha$ fluorescence intensity for the different precursors. While for the Cu–Zn–Sn–S system the Sn fluorescence intensity changes by less than 15% during the experiment, we find a strong decrease (Mo/SnS/CuS precursor) and a complete disappearance (Mo/Cu+Sn+S precursor) of the Sn signal for the Cu–Sn–S system. Al-
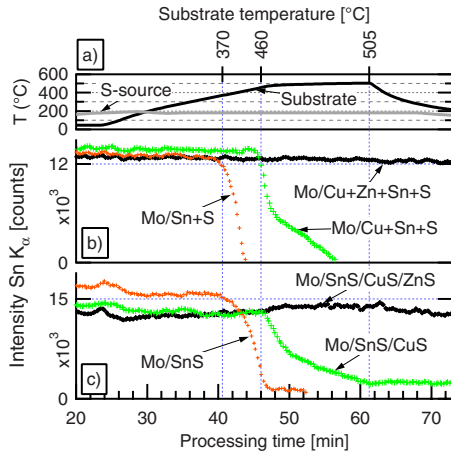
FIG. 2. (Color online) The intensity evolution of the Sn $K\alpha$ signal for the coevaporated precursors (b) and the sequentially evaporated precursors (c). The decrease in fluorescence intensity of the two tin sulfide films and the two copper tin sulfide films starts at similar temperatures. (a) gives the temperatures of the substrate and the S-source as functions of time.

though these two precursors have a different layout, the loss in Sn $K\alpha$ intensity starts at a similar temperature of about 460 °C. In the Sn+S and SnS precursors the diminishing of the Sn $K\alpha$ line starts at even lower temperatures of approximately 370 °C.

Figure 3 correlates the evolution of the fluorescence and diffraction signals for the precursor Mo/SnS/CuS. The decrease in Sn $K\alpha$ intensity at 470 °C coincides with the decrease in Cu_2SnS_3 and an increase in Cu_4SnS_4 diffraction intensity. At about 485 °C Cu_2SnS_3 disappears completely and also Cu_4SnS_4 intensity starts to decrease. The $Cu_{2-x}S$ diffraction signals augment with the decrease in Cu_4SnS_4 intensity.

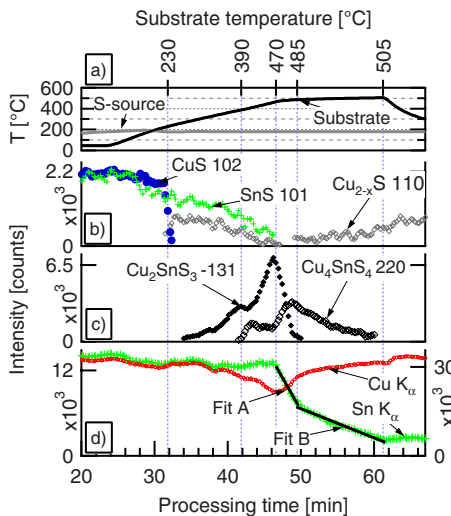This decrease in Sn $K\alpha$ intensity was not found for the

FIG. 3. (Color online) Signal intensities for the heating experiment on the precursor Mo/SnS/CuS. The signal intensities of prominent diffraction peaks of the binary phases (b), the ternary phases (c), and the fluorescence lines (d) are depicted. For the decrease in the Sn $K\alpha$ fluorescence intensity two regions were approximated by a linear curve fit. The slope of the first region was fitted to -1850 ± 70 counts/min (fit A) and of the second region to -400 ± 10 counts/min (fit B). The intensity immediately before the start of the first region was approximated to $13\,000 \pm 300$ counts. (a) gives the temperatures of the substrate and the S-source as functions of time.
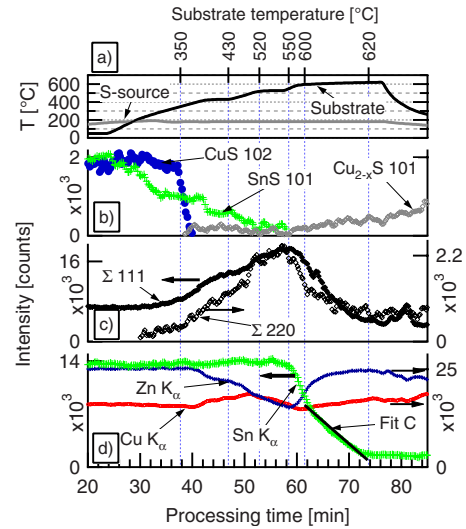

FIG. 4. (Color online) Signal intensities for the modified heating experiment on the precursor Mo/SnS/CuS/ZnS. The signal intensities of prominent diffraction peaks of the binary phases (b) and of the so-called Σ-signal are depicted [(c) the Σ-signal may be a sum of Cu_2ZnSnS_4, Cu_2SnS_3, and ZnS diffraction peaks]. (d) shows the evolution of the fluorescence lines of the different film elements. The decrease in the Sn $K\alpha$ fluorescence intensity in the temperature region between 600 and 620 °C was approximated by a linear curve fit. The slope was fitted to -630 ± 20 counts/min (fit C), and the starting intensity was approximated to $13\,800 \pm 400$ counts. (a) gives the temperatures of the substrate and the S-source as functions of time.

material system Cu–Zn–Sn–S in the standard heating process (see Fig. 2). In order to examine the thermal activation of Sn loss in this material system, a heating process with higher temperatures was applied to a Mo/SnS/CuS/ZnS precursor. Figure 4(a) shows the heating program for this experiment, which was based on three temperature dwells at approximately 420, 530, and 610 °C. Figure 4(b) depicts the intensities of diffraction peaks of the binary phases and Fig. 4(c) the intensities of two so-called Σ-signals, which may represent an overlap of the diffraction peaks of Cu_2ZnSnS_4, Cu_2SnS_3, and ZnS (sphalerite). The evolution of the fluorescence lines in Fig. 4(d) shows that also for the Cu–Zn–Sn–S system a significant decrease in the Sn $K\alpha$ signal is apparent for substrate temperatures exceeding 550 °C. At a constant temperature of approximately 610 °C the Sn fluorescence intensity decreases with a rate of 630 counts/min. With the Sn fluorescence signal also the intensities of the Σ-signals decrease while the $Cu_{2-x}S$ diffraction peak becomes stronger.

For the interpretation of the decreasing Sn $K\alpha$ signals it is advantageous to have information on the depth profile of the Sn share in the film before and after the drop in the Sn fluorescence signal in the film. Figure 5 depicts a SEM micrograph of the precursor Mo/SnS/CuS/ZnS after the standard heating program (where no decrease in Sn $K\alpha$ intensity was observed; see Fig. 2). A porous bottom layer and a top layer with large, Cu-rich grains can be discerned. In the bottom layer the Sn L fluorescence intensity exhibits a weak gradient toward the Mo backcontact. The micrograph in Fig. 6 is taken on the sample after the heating experiment with higher temperatures depicted in Fig. 4. The Sn signal is significantly lower than in Fig. 5 with a Sn gradient toward the backcontact.
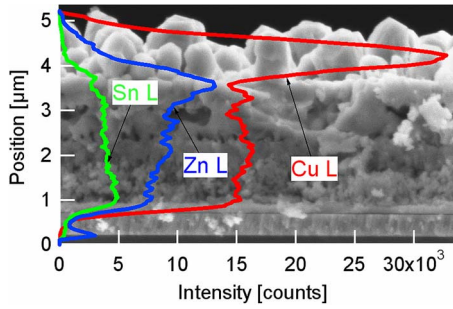
FIG. 5. (Color online) SEM cross section of the Mo/SnS/CuS/ZnS precursor after the standard heating process (see Fig. 2). The micrograph is overlaid by the integrated fluorescence signals of an EDX scan on the micrograph area. The Mo and S signals are omitted.

IV. DISCUSSION

The samples of all investigated material systems exhibit a significant decrease in the Sn $K\alpha$ fluorescence intensity when processed at sufficiently high temperatures. This effect can be caused by (i) varying absorption in the surrounding and covering material or by (ii) a loss of Sn from the layer.

For point (i) the absorption by Cu, Zn, and S has to be taken into account. Absorption of the incoming radiation above the Sn $K\alpha$ edge (29.2 keV), which can generate Sn $K\alpha$ fluorescence, as well as absorption of the generated Sn $K\alpha$ radiation ($E_{K\alpha1}=25.3$ keV, $E_{K\alpha2}=25.0$ keV), has to be considered. The cross section for the absorption of photons in this energy range can be found in table works.[19,20] With the cross section σ and the particle density per area ρ, the ratio of absorbed intensity to start intensity I_{abs}/I_0 in a layer of thickness x can be calculated according to Lambert–Beers law

$$\frac{I_{abs}}{I_0} = 1 - \exp(-\sigma\rho x). \tag{1}$$

A 2 μm thick layer of stoichiometric Cu$_2$ZnSnS$_4$ will have particle densities of 2.5×10^{18} at./cm^2 for Cu, 1.3×10^{18} at./cm^2 for Zn, and 5.0×10^{18} at./cm^2 for S. To calculate an upper limit for the absorption effect we assume that the Sn share of the film is completely accumulated in a layer at the back of the film. Sn $K\alpha$ photons emitted from this layer will be absorbed to 7% by the covering Cu, 4% by Zn, and 1% by S, resulting in a total attenuation of the Sn $K\alpha$
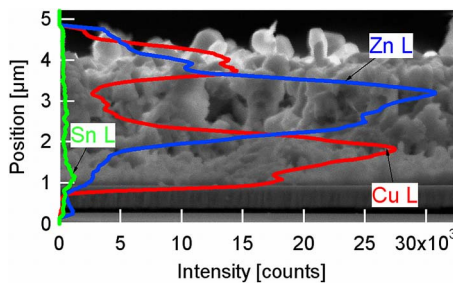

FIG. 6. (Color online) SEM cross section of the Mo/SnS/CuS/ZnS precursor after the heating process with high temperatures depicted in Fig. 4. Like in Fig. 5 the micrograph is overlaid by the integrated fluorescence signals of an EDX scan on the micrograph area. It is possible that covering copper sulfide grains delaminated during preparation of the cross section. The Mo and S signals are omitted.

TABLE III. Rate of the Sn loss from the precursors according to curve fits (A) and (B) in Fig. 3, fit (C) in Fig. 4, and Eq. (2). The temperatures are given as mean, rounded values for the interval of the curve fit. The phases in parentheses are assumed to be the origin of the Sn loss for the different processing stages and precursors, based on the XRD data in Figs. 3 and 4.

Precursor (phase with Sn loss)	Temperature (°C)	Loss rate [at./(cm^2 min)]
Mo/SnS/CuS (Cu$_2$SnS$_3$, fit A)	480	$(1.6 \pm 0.5)\times10^{17}$
Mo/SnS/CuS (Cu$_4$SnS$_4$, fit B)	495	$(3.4 \pm 1.1)\times10^{16}$
Mo/SnS/CuS/ZnS (Cu$_2$ZnSnS$_4$, fit C)	610	$(5.1 \pm 1.7)\times10^{16}$

radiation by 12%. The attenuation of the incoming photons above 29.2 keV, which excite the Sn $K\alpha$ radiation, will be lower than this due to lower cross sections for the interaction with Cu, Zn, and S at higher energies. Thus, the change in Sn $K\alpha$ fluorescence due to changing elemental distribution in the film is less than 24%. A generalized evaluation of the absorption of incoming and outgoing radiations based on first principles calculations can be found elsewhere[21] and will not be discussed here. A good empirical approximation of the influence of the elemental depth gradient on Sn fluorescence intensity can be made on the following basis: In the Mo/SnS/CuS/ZnS precursor Sn is, in fact, aggregated at the back of the film; the absorption by other constituents of the film should therefore be at a maximum. The EDX scan in Fig. 5 shows that Sn has distributed in the film during the annealing process at 500 °C. The Sn intensity during this process increases by less than 15%, according to the data in Figs. 2–4. A decrease in the Sn $K\alpha$ fluorescence intensity due to a change in the elemental depth distribution after this stage would therefore be limited to 15%, because the precursor layering represents the condition of maximum absorption by covering material. We therefore conclude that point (ii), the loss of Sn from the layer, is the main cause for the decrease in Sn $K\alpha$ fluorescence signal. This is confirmed by the disappearance of diffraction peaks of Sn-containing phases, the appearance of copper sulfides in Figs. 3 and 4, and the strong decrease in the Sn signal observed by EDX in Fig. 6.

If we neglect absorption effects the intensity of the Sn $K\alpha$ fluorescence signal depends linearly on the Sn amount in the layer. The evolution of the Sn amount $n_{Sn}(t)$ in the layers can then be derived from the starting Sn amount $n_{Sn,0}$, the starting fluorescence intensity $I_{Sn\,K\alpha,0}$, and the evolution of the fluorescence intensity $I_{Sn\,K\alpha}(t)$ by the linear relation

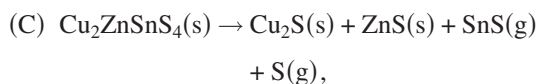$$n_{Sn}(t) = n_{Sn,0} \frac{I_{Sn\,K\alpha}(t)}{I_{Sn\,K\alpha,0}}. \tag{2}$$

With respect to absorption effects we assume a maximum error for the fluorescence intensity of 15%. Furthermore we approximate the error for the starting amount $n_{Sn,0}$, which is derived from the evaporation rates (see Table I for the values of $n_{Sn,0}$), to be less than 15%. With $n_{Sn,0}$ from Table I and the intensities from Figs. 3 and 4 we can calculate $n_{Sn}(t)$ according to Eq. (2). With the linear curve fits in Figs. 3 and 4 the Sn-loss rate can be approximated. The loss rates for the three different curve fits A–C are summarized in Table III.

For the precursor Mo/SnS/CuS two stages of Sn loss can be discerned and correlated to the observed crystalline phases (see the XRD data in Fig. 1). In a first stage at about 480 °C the Sn loss is coupled with a decrease in Cu_2SnS_3 diffraction intensity while Cu_4SnS_4 increases. In the second stage at about 495 °C Cu_2SnS_3 has vanished and the intensity of Cu_4SnS_4 decreases. We therefore conclude that in the first stage Sn is lost by the decomposition of Cu_2SnS_3 and in the second stage, significantly slower, by decomposition of Cu_4SnS_4. We found also for the precursor Mo/Cu+Sn+S two stages of Sn loss, which could be related to the phases Cu_2SnS_3 and Cu_4SnS_4, respectively.

For the precursor Mo/SnS/CuS/ZnS the development of phases during Sn loss is more difficult to scrutinize because of the possible overlap of ZnS, Cu_2SnS_3, and Cu_2ZnSnS_4 diffraction peaks. Nevertheless, with the results on the Sn loss from the ternary sulfides, it can be assumed that at 530 °C, before the Sn loss from the Mo/SnS/CuS/ZnS stack starts, no copper tin sulfides are present as they should have been decomposed already at lower temperatures. We therefore postulate that the Sn loss from these layers can be traced back to the decomposition of Cu_2ZnSnS_4.

We still did not address the question in which form Sn is desorbed from the films. According to known data for the Sn-vapor pressure[22] it can be excluded that elemental Sn is evaporated from the films at a significant rate; the evaporated particles will therefore be molecules. In the material system Cu–Zn–Sn–S the Sn-containing compounds can be tin sulfides, copper tin sulfides, or copper tin alloys.[23,24] The evolution of the Cu $K\alpha$ fluorescence during the heating experiment on the precursor Mo/SnS/CuS in Fig. 3 indicates that there is no loss of Cu from the films. We therefore conclude that the Sn loss is due to the evaporation of tin sulfide. This is also affirmed by the experimental finding in Fig. 2 where the films of the material system Sn–S show Sn loss at lower temperatures as the other material systems. The high vapor pressure of tin sulfides has been the subject of several scientific publications.[25–27] By mass spectrometric measurements the molecules in the gas phase could be identified as mainly SnS.[28] The sulfur rich tin sulfides SnS_2 and Sn_2S_3 decompose firstly by desorbing sulfur and evaporating SnS at higher temperatures.[27] We therefore conclude that in our experiments SnS is evaporated and suggest the following decomposition reactions (for simplification $Cu_{2-x}S$ is approximated by Cu_2S):

(A) $2Cu_2SnS_3(s) \rightarrow Cu_4SnS_4(s) + SnS(g) + S(g)$,

(B) $Cu_4SnS_4(s) \rightarrow 2Cu_2S(s) + SnS(g) + S(g)$,

(C) $Cu_2ZnSnS_4(s) \rightarrow Cu_2S(s) + ZnS(s) + SnS(g)$
$$+ S(g),$$

where (s) denotes a solid state phase and (g) a gaseous phase. These reactions comply very well with the observed evolution of phases during Sn loss.

It is very plausible to assume that the Sn loss and the formation of the solid decomposition products start at the top of the film, where the gaseous phase desorbs. This is con-
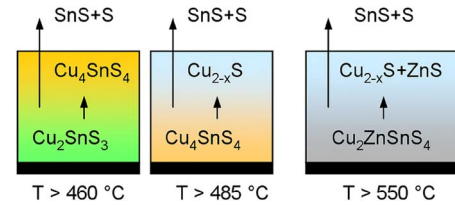

FIG. 7. (Color online) Schematic representation of the decomposition of different Sn-containing phases in thin films. The temperatures at the bottom correspond to the starting points of the decomposition as they were found in the experiments of Figs. 3 and 4.

firmed by the EDX depth profile in Fig. 6. On this basis a schematic of the Sn loss from thin films of the different phases is drawn in Fig. 7.

Although there are some reports in literature about annealing experiments on Cu–Zn–Sn–S films at temperatures of 550 °C and above[29–31] a significant Sn loss from these films has never been observed. All of these cited annealing experiments were carried out in N_2+H_2S atmosphere. For evaporation in vacuum the maximum evaporation rate dn/dt per area A can be expressed by kinetic gas theory (Hertz–Knudsen equation[32,33]) to

$$\frac{dn}{Adt} = \sqrt{\frac{1}{2\pi m k_B T}} p^*, \tag{3}$$

where m is the mass of the evaporant particles, k_B is the Boltzmann constant, and p^* is the equilibrium vapor pressure of the evaporating species at the temperature T. If the evaporation process is not carried out in vacuum but in a gas atmosphere the kinetic gas theory approach of the Hertz–Knudsen equation is not applicable anymore. The evaporant particles collide with the surrounding gas particles and the evaporation will be controlled by diffusion and convection in the surrounding gas phase.[34] As a general rule it can be stated, also on the basis of several experimental works,[32,35,36] that due to this effect the evaporation rate in an inert gas atmosphere is always lower than in vacuum. We argue therefore that the N_2+H_2S atmosphere of the experiments cited above[29–31] explains the missing Sn loss in those cases.

V. CONCLUSION

By the application of *in situ* XRD and XRF we could show that for a pressure of 1×10^{-2} Pa and temperatures above 350 °C thin films of the material systems Sn–S, Cu–Sn–S, and Cu–Zn–Sn–S evaporate SnS. Ternary (Cu_2SnS_3 and Cu_4SnS_4) and quaternary (Cu_2ZnSnS_4) phases decompose and copper sulfides and zinc sulfides remain as solid phases in the film. The evaporation rate from the different phases increases according to the sequence $Cu_2ZnSnS_4 \rightarrow Cu_4SnS_4 \rightarrow Cu_2SnS_3 \rightarrow SnS$. For Cu_2ZnSnS_4 a SnS loss with significant rates occurs at temperatures of 550 °C and above. These high temperatures are usually applied to the deposition of $Cu(In,Ga)Se_2$ absorber films and appear to be beneficial for device quality.[37] For the PVD of Cu_2ZnSnS_4 in this temperature region the loss of SnS from the layers has to be considered. An additional inert gas atmosphere can suppress material transport through the gas phase and therefore reduce SnS evaporation from the substrate. A feasible

method for the deposition of Cu_2ZnSnS_4 thin films may therefore include thin film deposition by PVD at temperatures below 550 °C and a subsequent annealing step in inert gas atmosphere to improve crystal quality.

ACKNOWLEDGMENTS

[1] K. Ito and T. Nakazawa, Jpn. J. Appl. Phys., Part 1 **27**, 2094 (1988).

[2] H. Katagiri, K. Jimbo, S. Yamada, T. Kamimura, W. S. Maw, T. Fukano, T. Ito, and T. Motohiro, Appl. Phys. Express **1**, 041201 (2008).

[3] S. R. Hall, J. T. Szymanski, and J. M. Stewart, Can. Mineral. **16**, 131 (1978).

[4] J. Paier, R. Asahi, A. Nagoya, and G. Kresse, Phys. Rev. B **79**, 115126 (2009).

[5] S. Chen, X. G. Gong, A. Walsh, and S. H. Wie, Appl. Phys. Lett. **94**, 041903 (2009).

[6] S. Schorr, Thin Solid Films **515**, 5985 (2007).

[7] T. M. Friedlmeier, H. Dittrich, and H. W. Schock, Proceedings of the 11th International Conference on Ternary and Multinary Compounds (ICTMC), Salford, 1997 (unpublished), p. 345.

[8] T. Tanaka, D. Kawasaki, M. Nishio, Q. Guo, and H. Ogawa, Phys. Status Solidi C **3**, 2844 (2006).

[9] A. Weber, H. Krauth, S. Perlt, B. Schubert, I. Kötschau, S. Schorr, and H. W. Schock, Thin Solid Films **517**, 2524 (2009).

[10] K. Oishi, G. Saito, K. Ebina, M. Nagahashi, K. Jimbo, W. S. Maw, H. Katagiri, M. Yamakazi, H. Araki, and A. Takeuchi, Thin Solid Films **517**, 1449 (2008).

[11] M. A. Contreras, M. J. Romero, and R. Noufi, Thin Solid Films **511–512**, 51 (2006).

[12] Ch. von Klopmann, J. Djordjevic, and R. Scheer, J. Cryst. Growth **289**, 113 (2006).

[13] K. Koto and N. Morimoto, Acta Crystallogr., Sect. B: Struct. Crystallogr. Cryst. Chem. **26**, 915 (1970).

[14] T. Chattopadhyay, J. Pannetier, and H. G. von Schnering, J. Phys. Chem. Solids **47**, 879 (1986).

[15] M. Onoda, X. Chen, M. Sato, and H. Wada, Mater. Res. Bull. **35**, 1563 (2000).

[16] P. S. Jaulmes, J. Rivet, and P. Laruelle, Acta Crystallogr., Sect. B: Struct. Crystallogr. Cryst. Chem. **33**, 540 (1977).

[17] M. Oliveria, R. K. McMullan, and B. J. Wünsch, Solid State Ionics **28–30**, 1332 (1988).

[18] F. Hergert and R. Hock, Thin Solid Films **515**, 5953 (2007).

[19] D. C. Creagh and J. H. Hubbell, *X-Ray Absorption (or Attenuation) Coefficients*, International Tables for Crystallography Vol. C (Kluwer, Dordrecht, 1992), Sec. 4.2.4, pp. 189–206.

[20] J. H. Scofield, "Theoretical photoionization cross sections from 1 to 1500 keV," LLNL Report No. UCRL-51326, 1973.

[21] R. Mainz, "In-situ analyse und wachstum photovoltaischer absorber mit bandlückengradienten," Ph.D. thesis, Free University Berlin, 2008.

[22] F. Geiger, C. A. Busse, and R. I. Loehrke, Int. J. Thermophys. **8**, 425 (1987).

[23] G. H. Moh, Chem. Erde **34**, 1 (1975).

[24] I. D. Olekseyuk, I. V. Dudchak, and L. V. Piskach, J. Alloys Compd. **368**, 135 (2004).

[25] A. W. Richards, Trans. Faraday Soc. **51**, 1193 (1955).

[26] H. Wiedemeier and J. S. Csillag, Thermochim. Acta **34**, 257 (1979).

[27] V. Piacente, S. Foglia, and P. Scardala, J. Alloys Compd. **177**, 17 (1991).

[28] R. Colin and J. Drowart, J. Chem. Phys. **37**, 1120 (1962).

[29] H. Katagiri, Thin Solid Films **480-481**, 426 (2005).

[30] T. Kobayashi, K. Jimbo, K. Tsuchida, S. Shinoda, T. Oyanagi, and H. Katagiri, Jpn. J. Appl. Phys., Part 1 **44**, 783 (2005).

[31] K. Jimbo, R. Kimura, T. Kamimura, S. Yamada, W. S. Maw, H. Araki, K. Oishi, and H. Katagiri, Thin Solid Films **515**, 5997 (2007).

[32] H. Hertz, Ann. Phys. **253**, 177 (1882).

[33] M. Knudsen, Ann. Phys. **352**, 697 (1915).

[34] C. Boyadjiev and B. Boyadjiev, Int. J. Heat Mass Transfer **46**, 1679 (2003).

[35] G. R. Fonda, Phys. Rev. **21**, 343 (1923).

[36] E. Fromm, Metall. Trans. A **9A**, 1835 (1978).

[37] C. A. Kaufmann, R. Caballero, T. Unold, R. Hesse, R. Klenk, S. Schorr, M. Nichterwitz, and H. W. Schock, Sol. Energy Mater. Sol. Cells **93**, 859 (2009).